Experimental Thermal and Fluid Science 167 (2025) 111493

Contents lists available at ScienceDirect

Experimental Thermal and Fluid Science

journal homepage: www.elsevier.com/locate/etfs

Characterization of splashing and regime thresholds for oblique droplet impact on thin wall films

Jonathan Lukas Stober [a],*, Maurizio Santini [b], Kathrin Schulte [a]

[a] Institute of Aerospace Thermodynamics, University of Stuttgart, Pfaffenwaldring 31, Stuttgart, 70569, Germany
[b] Department of Engineering and Applied Sciences, University of Bergamo, Viale G. Marconi 5, Dalmine, 24044, Italy

ARTICLE INFO

Keywords:
Droplet impact
Oblique
Thin wall film
Splashing
Regime thresholds

ABSTRACT

This study experimentally investigates oblique droplet impacts on thin wall films, providing new insights into crown formation, splashing types, and threshold modelling. Different splashing types were identified by varying the impact angle α and Weber number We, keeping the film thickness $\delta = 0.22$ and fluid (isopropanol) constant. The splashing types include secondary droplet ejection only from the front or only from the sides of the crown, splashing caused by crown-film interaction, and 90°-like splashing. Combinations of these mechanisms, such as simultaneous front and side splashing, were also observed, as their triggering mechanisms are independent and allow for a superposition of regimes. A regime map and threshold formulations were developed to describe the distinct splashing types. The front splashing limit lies at $\cos(\alpha)\,We = 128$, which reveals that the $\cos(\alpha)$ is the relevant physical quantity beside the Weber number. Side splashing depends solely on the wall-normal Weber number ($We_n = 425$). Crown-film interactions occur below $\alpha < 60°$ if the Weber number is high enough, while splashing similar to that seen when $\alpha = 90°$ is observed if the impact angle exceeds $\alpha > 81°$.

1. Introduction

Droplet impacts on a thin film of the same liquid are fundamental to numerous technical and environmental processes. Some examples are spray cooling of electronic components [1], medical inhalers, the water recovery unit of a water-enhanced turbofan [2], and wall-impingement of fuel sprays in engines [3]. In these applications, droplets impact with different velocities and angles, often on a wetted wall. If the impact energy is high enough, a crown forms from which secondary droplets detach, called splashing [4]. To improve the efficiency of the above-mentioned applications, it is crucial to understand the mechanisms of splashing and the thresholds for it to happen.

The normal droplet impact onto a wall film of the same liquid has been investigated thoroughly [4–8]. It is defined by the droplet diameter D, its velocity U, the film thickness h and the liquid properties, density ρ, surface tension σ, and dynamic viscosity μ. The impact parameters can be combined in non-dimensional numbers. Typically, the Weber number $We = \rho D U^2/\sigma$ and the Ohnesorge $Oh = \mu/\sqrt{\rho D \sigma}$ or Reynolds number $Re = \rho D U/\mu$ are used, as well as the non-dimensional film thickness $\delta = h/D$. The non-dimensional time $\tau = tU/D$ describes the temporal development with the time t after the first contact of the droplet with the wall film.

Splashing can be further classified depending on when and from which part of the impact structure the secondary droplets detach. During *prompt splashing*, many tiny droplets are generated right after the impact ($\tau < 1.0$) when the crown starts to form; see the sketch in Fig. 1a. Prompt splashing occurs for low Ohnesorge numbers $Oh \approx 0.0022$ *e.g.* water [4]. *Crown splashing* describes the separation of secondary droplets at a later time, which occurs from fingers that develop at the crown's rim or directly from the rim [4] (Fig. 1b). When the crown falls back onto the film, the fluid flows back to the centre of impact where a Worthington jet can form [9], and, if the energy of the back flow is high enough, secondary droplets detach from it, which is called *Worthington splashing* (Fig. 1c).

A splashing factor K that combines the We and Oh by $K = We\,Oh^{-0.4}$ is suitable to describe the splashing/deposition limit for impacts on dry walls [5] as well as impacts on wall films [4]. A threshold value K_L separates deposition ($K < K_L$), where no secondary droplets are generated, from splashing ($K > K_L$). Cossali et al. [4] conducted a large experimental study for normal droplet impacts on thin films ($0.1 < \delta < 1$) under varying conditions and derived a model for the threshold value $K_L = 2100 + 5880\,\delta^{1.44}$ that describes the dependency of splashing on the non-dimensional film thickness δ.

In practical applications, many droplets impact a wetted wall obliquely. The oblique impact is defined by the same parameters as the

* Corresponding author.
E-mail address: jonathan.stober@itlr.uni-stuttgart.de (J.L. Stober).

https://doi.org/10.1016/j.expthermflusci.2025.111493
Received 4 March 2025; Received in revised form 31 March 2025; Accepted 6 April 2025
Available online 16 April 2025
0894-1777/© 2025 The Authors. Published by Elsevier Inc. This is an open access article under the CC BY license (http://creativecommons.org/licenses/by/4.0/).

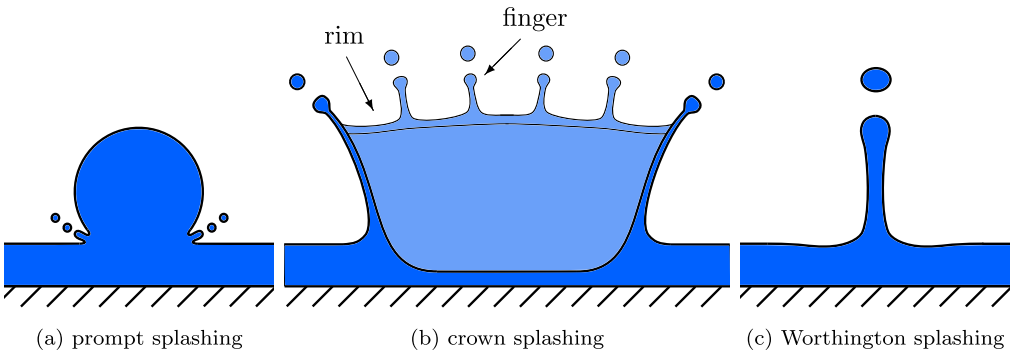

Fig. 1. Sketch of different splashing types occurring during normal droplet impact on a thin wall film.

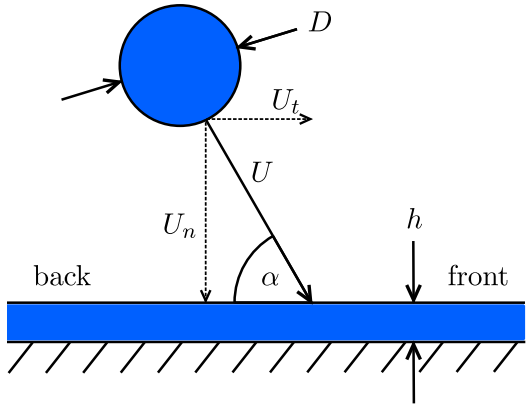

Fig. 2. Sketch of an oblique droplet impact onto a wall film.

normal impact, but with the impact angle α as an additional parameter, as sketched in Fig. 2. The impact velocity U consists of a component tangential to the wall film surface U_t and a component normal to the film U_n. The Weber number We of the impact is calculated with the total velocity U. For the oblique impact, there are also the tangential Weber number $We_t = \rho D U_t^2/\sigma$ and the wall-normal Weber number $We_n = \rho D U_n^2/\sigma$, which are calculated with U_t and U_n, respectively. The following trigonometric relations apply for the velocities and Weber numbers: $\sin(\alpha) = U_n/U$; $\sin(\alpha)^2 = We_n/We$; $We_t + We_n = We$.

Compared to normal impacts, oblique droplet impacts have received considerably less attention, leaving many questions regarding splashing morphologies and the threshold description unresolved for impacts on thin films. An oblique impact onto a horizontal quiescent wall film is challenging to achieve experimentally, as the droplet has to be generated with a velocity component tangential to the wall film.

Okawa et al. [10] investigated oblique droplet impacts experimentally with water by generating droplets with a flat spray nozzle and isolating a single droplet with a small orifice plate. They varied the film thickness (thick film/deep pool, $2 < \delta < 30$), the impact angle ($15° < \alpha < 79°$), and the impact velocity to determine a splashing threshold and to characterize the size and number of secondary droplets. During the impact, an asymmetric liquid sheet in the shape of a ship's prow forms from which the secondary droplets detach. A deposition/splashing threshold around $K_L \approx 2\,100$ was found if the total component of the impact velocity is used to calculate K and as long as the impact angle $\alpha > 30°$. For lower impact angles, splashing is shifted to higher impact factors, and for $\alpha < 15°$, splashing is not observed at all. The mass and size of the secondary droplets change significantly with the impact angle. Due to small primary droplets ($D \lessapprox 1$ mm), experiments that investigate the thin film regime ($\delta < 1$) were not possible. Furthermore, the resulting crown is comparably small and, considering the high-speed imaging technology at that time, only general observations about the crown morphology and detachment process of secondary droplets could have been made.

In a more recent experimental study, Bao et al. [11] conducted oblique impacts ($70° < \alpha < 90°$) on thin films ($\delta = [0.17, 0.33, 0.5]$) by deflecting the droplets with a horizontal airflow. They varied the droplet shape of the primary droplet by varying the horizontal and vertical droplet diameters (D_h, D_v) and provided detailed insights into the crown development and splashing process. For impacts of spherical droplets, the asymmetric crown shape was described as a bevelled round tube. Droplets detach from the front part of the crown (in the direction of impact) from multiple fingers if the impact energy is high enough. A ship prow-like crown in the front direction was observed for vertically spheroidal droplets ($D_v > D_h$), which promote splashing at the front. In contrast, horizontal spheroidal droplets ($D_h > D_v$) lead to a more symmetric crown where secondary droplets detach at the sides of the crown. As the study was focused on droplet shape, no large variations in impact angle or Weber number were applied, and no splashing threshold was derived.

In another recent study, Stober et al. [12] conducted oblique impact experiments ($\alpha = 60°$) on a thin wall film ($\delta = 0.22$) with varying the Weber number in a broad range ($250 < We < 700$). The impact was recorded with two synchronized high-speed cameras to provide detailed information about crown development and the subsequent splashing process. An asymmetric crown was observed with a single central finger growing on the front part, while on the rest of the crown's rim, cusps form. On the back side, the crown is bent inwards initially. One or multiple secondary droplets detach from the finger at the front. For an increase in Weber number, an interaction of the early crown at the front with the wall film can be observed. This causes the rim to rupture and multiple fingers to form on the front part of the crown leading to splashing with more and smaller secondary droplets. Furthermore, the study showed that splashing occurs for lower Weber numbers calculated with the total impact velocity than in a normal impact case. However, a threshold was not presented, as the Weber number was not low enough for deposition.

To the best of the authors' knowledge, the three above-presented studies are the only ones that have investigated an oblique droplet impact on a horizontal and quiescent wall film experimentally. However, other publications discuss impacts on deep pools, for example Gielen et al. [13], which investigates splashing thresholds for varying impact angles. They distinguish between one-sided splashing and omni-directional splashing. For oblique impacts with $\alpha > 50°$, the threshold for one-sided splashing is lower than for the normal impact, and the threshold for omni-directional splashing is higher. Omni-directional splashing was only observed for slightly oblique impacts with $\alpha > 70°$. All splashing was prompt splashing in that study, due to the low Ohnesorge number and water being used as liquid.

Liang et al. [14] and Cheng et al. [15] investigated oblique droplet impacts on thin films by dropping the droplet vertically from above but inclining the wall. To achieve a stable wall film that does not flow,

only very thin films $\delta < 0.1$ and impact angles close to perpendicular can be investigated. Furthermore, the film thickness depends on the inclination angle, and an independent variation of these parameters is not possible.

A droplet impact onto a flowing wall film is similar to an oblique impact. If the wall moves with the film and if the influence of the surrounding air is neglected, an oblique droplet impact on a quiescent film, and a normal impact on a moving film is Galilean-equivalent. However, if the wall is not moving, a velocity gradient develops inside the wall film. Besides that, flowing films often have a wavy surface. Both effects make it difficult to transfer observations made on flowing wall films to oblique impacts on a quiescent film. Furthermore, due to the design of the experiment, film thickness and film velocity can often not be changed independently from each other, which makes it impossible to separate effects caused by thickness variation or the oblique nature. Several experimental studies have been conducted with flowing wall films [16–21]. Among these, Gao and Li [16] investigated the normal impact on a radially, horizontally flowing thin film ($\delta < 0.4$). They observed earlier splashing on the front side compared to that for a steady film, and they derived a formulation for the splashing limit. The threshold is expressed with a modified Weber and Reynolds number that takes the film velocity and thickness into account, $We_m = \rho/\sigma(DU^2+hU_f^2)$, with the film velocity U_f. This is done equivalently for the Reynolds number. This modification corresponds to a Weber number that is weighted of the wall-normal Weber number and the total Weber number calculated with the film velocity and droplet velocity as in an oblique impact. The weights depend on the non-dimensional film thickness δ. Also in that study, waves were observed on the wall film, which could shift the splashing threshold. Furthermore, the influences of the film thickness and velocity were not investigated separately.

Besides experimental work, there are numerical studies that describe crown morphologies, splashing mechanisms, or splashing thresholds. An initially inwards bent crown on the back side, as observed in the experiments of Stober et al. [12], was also observed numerically in different studies [22–26]. An explanation for this phenomenon was given by Stober et al. [25] who conducted highly resolved Direct Numerical Simulation and called it *oblique mechanism of crown formation*. Splashing occurring only on the front side, while the back side of the crown stays stable, has been described numerically in several publications [22–24,27]. Cheng et al. [27] conducted a large parameter study varying the impact angle ($\alpha = [45°, 60°, 75°, 90°]$), film thickness ($\delta = [0.1, 0.2, 0.3, 0.4]$), and Weber and Ohnesorge number. A splashing threshold was found to be independent of the impact angle α when using the total Weber number. The exponents for the splashing factor K were adapted to $K = We\,Oh^{-0.66}$, and a $K_L = 3966$ was derived. It has to be noted that the fitting was done with only three data points for the Ohnesorge number. Furthermore, the crown morphology in the DNS does not show a typical rim as observed in experiments, and splashing happens chaotically from the crown, which could hint at an under-resolved simulation. The onset of splashing is highly sensitive to grid resolution [28], which makes the derived splashing threshold questionable.

The above overview of the current literature highlights several gaps in understanding. First, detailed descriptions of crown morphology development and splashing types for oblique impacts, especially for thin films $\delta < 1$, are still lacking. Second, it remains an open question which physically quantities best describe the deposition/splashing threshold for oblique impacts — whether total or normal Weber numbers (We, We_n), the impact angle (α), or another parameter.

This publication aims to address these questions through an extensive experimental parameter study systematically varying the impact angle and Weber number while keeping the film thickness and fluid properties (*i.e.* Ohnesorge number) constant. Impact morphology is recorded from three perspectives (side, front, and top view) providing detailed insights into the splashing mechanisms. Section 2 explains the experimental methodology. Section 3 presents and discusses the results, including a regime map of the different splashing types, detailed characterization of each regime, and proposed thresholds for the regime boundaries. Finally, Section 4 summarizes the findings and provides conclusions.

2. Experimental method

The experimental setup and procedure are similar to those in our previous experimental study [12], where further details can be found. The key techniques, such as the droplet generator (Section 2.1) and the camera setup (Section 2.2), as well as modifications of the setup are explained in the following. Furthermore, the investigated parameter space of impact conditions is presented (Section 2.3).

2.1. Droplet generator

To achieve an oblique droplet impact onto a quiescent and horizontal wall film, the droplets need to be ejected from a droplet generator with a horizontal velocity component. As gravity adds a vertical velocity component, the droplet impacts obliquely following a parabolic trajectory. The droplet generator consists of a needle, supplied with isopropanol, that moves along a rail. The needle undergoes rapid deceleration in the front turning point, causing some of the liquid to eject due to its inertia. One or multiple droplets detach with a horizontal velocity component. The droplet generator's kinematics are precisely controlled using an in-house Visual Basic program. Details about the droplet generator can be found in Santini et al. [29] and Stober et al. [12].

The mounting position of the droplet generator, *i.e.* distance and height to the impact area, as well as its inclination can be adjusted. The mass flow rate and velocity are fine-tuned to ensure repeatable detachments from the needle and to achieve a specific impact location and impact conditions (D, U, α). This setup allows for a wide range of independent variations of the impact angle and velocity.

2.2. Camera setup and film thickness measurement

The impact process is recorded from three perspectives, a side view (blue in Fig. 3), a front view (red), and a top view (green), which is newly added for this study. The shadowgraphy technique is applied to visualize the crown development and detachment of secondary droplets. An LED and a lens are used for background illumination. The imaging setup consists of two identical high-speed cameras (Photron SA-X2) with the same camera objective (Optem Fusion: extension tube + zoom module + lower lens), which record from two perspectives synchronized. The side view can be combined with either the front view or the top view as shown schematically in Fig. 3a and 3b. The cameras record with a frame rate of 12 500 fps and a total resolution of $1\,024 \times 1\,024\,\mathrm{px}^2$, which together with the camera objective leads to a magnification factor of 24 µm/px.

Fig. 3 shows example recordings of all three perspectives of an oblique impact experiment to explain the different perspectives and to define regions of the crown and quantities that are used in the next sections. The side view (blue) records the crown from the side, and the droplet approaches the film obliquely from the top left. In the front view (red), the impacting droplet moves towards the observer, and in the top view (green), it enters the view from the left. The part of the crown which develops in the direction of the impact (*i.e.* direction of tangential velocity component U_t) is referred to as the *front* part of the crown. It is located on the right side in the side and top view and in the middle of the front view. Equivalently, the crown which develops against the direction of impact is referred to as the *back* part of the crown, visible in the side and top view and usually not visible in the front view, as the front crown is higher. The *side* part of the crown describes the region that develops sideways (*i.e.* perpendicular) to the direction of impact and is visible in all three views.

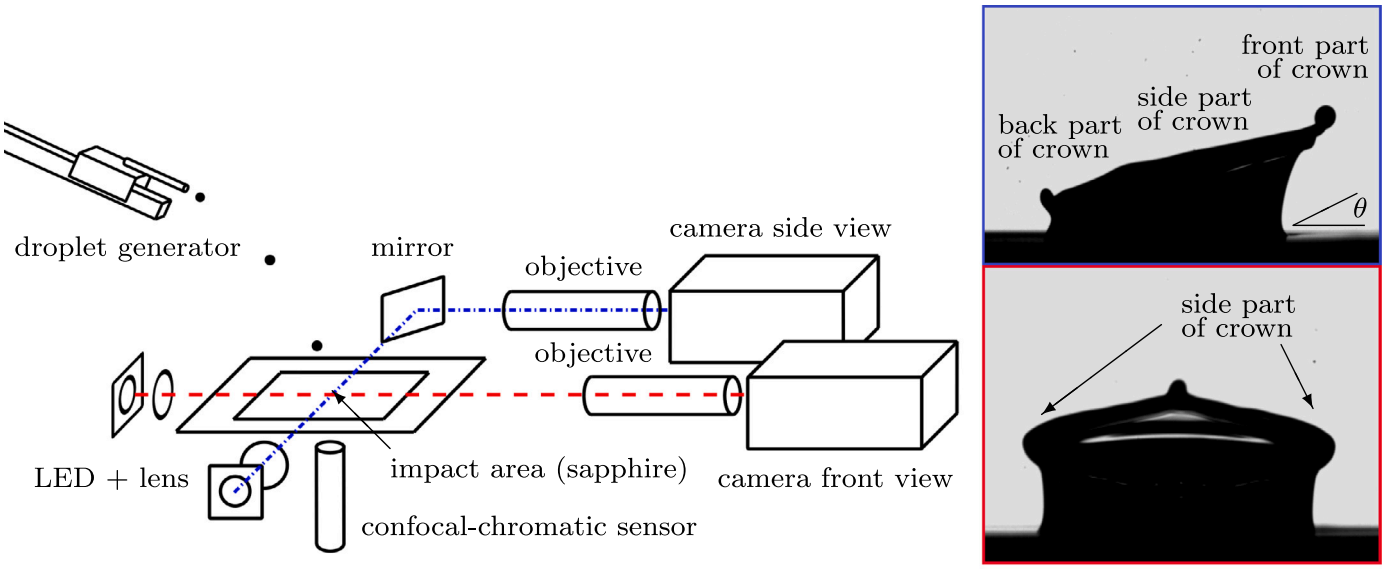

(a) side and front view

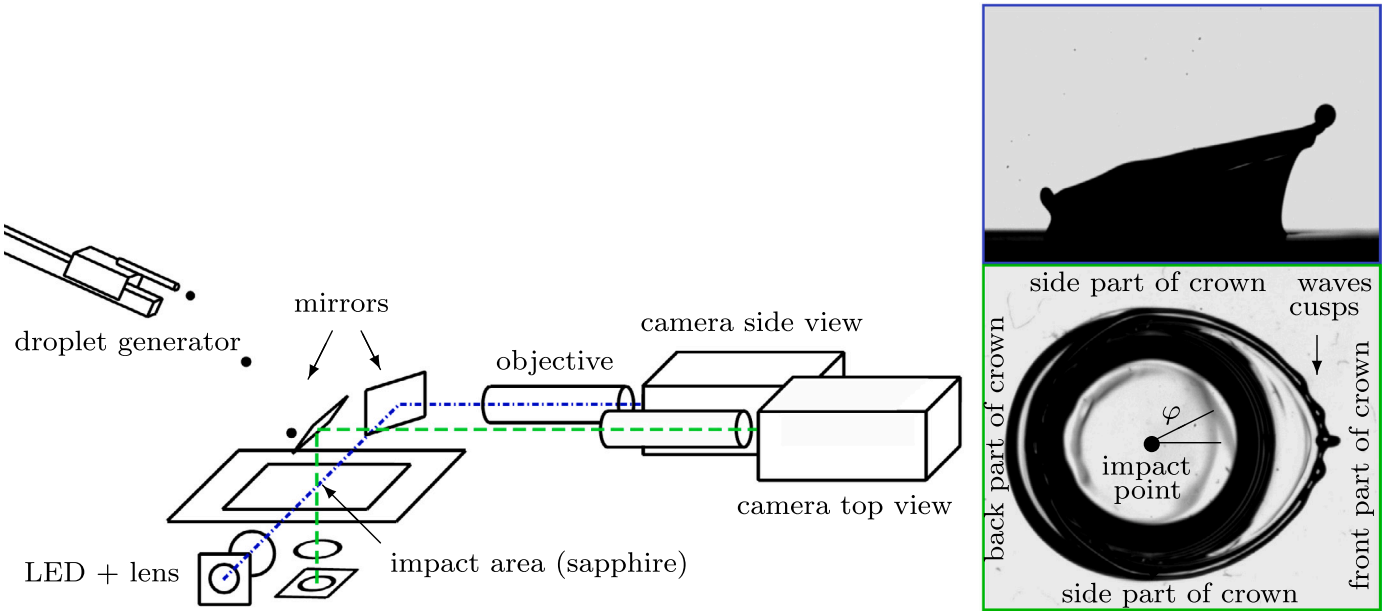

(b) side and top view

Fig. 3. Schematic sketch of the camera setup for the synchronized high-speed video recordings and examples recordings highlighting important parts of the crown (side and front views Exp. No. 5, top view Exp. No. 6 at $\tau = 5.7$.

The azimuth angle φ is introduced to describe positions in the crown and the direction of the trajectories of secondary droplets. It is drawn in the top view, and $\varphi = 0°$ is defined in the direction of impact. The elevation angle θ is marked in the side view and describes the trajectories of secondary droplets in reference to the film surface. With a combination of φ and θ, every direction can be described.

The impact surface is a 2 mm thick sapphire plate (50 mm × 50 mm) to which a thin film of isopropanol is applied. The liquid is held by its surface tension on the edge of the plate and its thickness is measured with a confocal–chromatic sensor (Micro Epsilon sensor and controller: IFS2405-3, IFC2421MP) from below through the sapphire. Details about the confocal–chromatic distance measuring technique can be found in Ruprecht et al. [30]. In this setup, a sensor with a 3 mm measuring range is used combined with a multi-peak controller that can detect up to six interfaces, which is an improvement compared to the previous setup [12]. The sensor is positioned such that the full sapphire plate and the liquid film are within the measurement range. With that, the thickness of the film can be measured more accurately than in the previous setup. The measurement uncertainty for the initial wall film thickness is only $\Delta h_f = 2.0\,\mu m$ (0.7%).

The side view combined with the front view is used to differentiate between the distinct splashing types described in Section 3, and most experiments were conducted with this setup. In that case, the thickness is measured continuously during the experiment with the described uncertainty. Some selected experiments were recorded with the side combined with the top view to provide further understanding of the splashing process. In that case, the LED and lens for the background illumination have to be placed below the sapphire plate. The film thickness is measured first, the sensor is removed afterwards, and the lighting is installed. Subsequently, the experiment is conducted. This time difference causes a deviation of the measured film thickness from the actual thickness present during the experiment. The change in

Table 1
Density ρ, surface tension (in air) σ, and dynamic viscosity μ of isopropanol at 25 °C±2 K, extracted from Dortmund Data Base [31].

ρ [kg/m^3]	σ [mN/m]	μ [mPa s]
781.5 ± 2.8	20.99 ± 0.27	2.056 ± 0.18

Table 2
Impact conditions and splashing type for the selected experimental recordings shown in this study.

Exp. No.	We [–]	α [°]	δ [–]	Oh [–]	Spl. Type
1	553	82.4	0.218	0.0138	90L
2	703	81.8	0.219	0.0129	90L
3	489	75.5	0.228	0.0139	SO
4	478	76.3	0.234	0.0131	SO
5	395	64.5	0.216	0.0131	sFO
6	460	62.0	0.203	0.0125	sFO
7	486	61.8	0.222	0.0137	mFO
8	448	62.2	0.202	0.0126	mFO
9	284	53.6	0.209	0.0133	FO
10	539	67.6	0.214	0.0136	F+S
11	601	70.0	0.215	0.0130	F+S
12	469	54.2	0.233	0.0131	I
13	656	59.1	0.201	0.0128	I+S
Uncertainty	±16	±0.6	±0.005	±0.001	

thickness due to evaporation was determined empirically. The time between measurement and experiment was measured and limited to one minute. With that, the measured film thickness can be corrected by the empirically estimated rate of change in film thickness. This however introduces additional uncertainties leading to a total uncertainty of $\Delta h_f = 9.0\,\mu$m (3%) for experiments recorded with the top view.

2.3. Impact conditions

The impact conditions (droplet diameter D, velocity U, and impact angle α) are determined with an in-house Matlab program from the side view recordings. The uncertainty for the droplet diameter was determined to $\Delta D = 33\,\mu$m (2.2%) considering uncertainties in the processing routine, motion blur, and uncertainties in the magnification factor. For the impact velocity and impact angle, the uncertainties are quantified equivalently to $\Delta U = 0.03$ m/s ($\approx 1\%$) and $\Delta\alpha = 0.6°$ ($\approx 1\%$) respectively. The fluid properties of isopropanol, which is used as droplet and film liquid, are summarized in Table 1. Uncertainties in the fluid properties arise from temperature variations in the laboratory $\Delta T = 3$ K. The uncertainties of the derived quantities are calculated with the Gaussian law of error propagation and are given in Table 2.

In this study, the impact angle α and Weber number We are varied in a broad range. Impact angles from $\alpha = 50°$ to $\alpha = 83°$ and $\alpha = 90°$ were investigated with Weber numbers ranging from $We = 180$ up to $We = 700$. The other impact parameters (δ, Oh, and fluid properties) were kept constant. The non-dimensional film thickness was between $0.20 \leq \delta \leq 0.24$. The droplet diameter can vary in the range of $1.3\,\text{mm} \leq D \leq 1.7\,\text{mm}$ which leads to an Ohnesorge number $Oh = \mu/\sqrt{\rho D\sigma}$ within a range $0.012 \leq Oh \leq 0.014$.

Table 2 summarizes the impact conditions of selected experiments.

3. Results and discussion

Fig. 4 provides an overview of all conducted experiments dependent on the total impact Weber number We and the impact angle α. Each dot represents a single experiment, and the different colours indicate different splashing types, which are described in the following sections. Many experiments under similar conditions are conducted to prove the reproducibility of the observed splashing types and to obtain a statistically valid database. In total, over 600 experiments were recorded and evaluated. From this plot, distinct areas and regime borders can be identified. This demonstrates the reproducibility of the impact outcomes and the quality of the experimental setup and procedure. Furthermore, this proves that the data provides a solid source for the mathematical description of regime thresholds.

In the next sections, high-speed camera recordings of the different splashing types are shown from multiple perspectives to explain the development of the crown, rim, and fingers in detail, as well as the mechanisms that lead to the separation of secondary droplets. The range of impact conditions under which they occur are explained, and threshold formulations are derived that separate the different regimes in the two-dimensional parameter space of the Weber number We and impact angle α.

3.1. 90°-like splashing (90L)

For a droplet impact under $\alpha = 90°$, the Worthington splash and regular crown splash are typical splashing types [4], as sketched in Fig. 1 in the introduction (Section 1). In the case of an oblique impact, both phenomena are observed similarly as long as the impact angle is close to 90°; see the yellow dots in Fig. 4. The Worthington jet is generated by a reverse flow to the centre of the impact caused by the receding of the crown. For an oblique impact, the receding happens first at the back and later at the front. The strength of the flow caused by the receding crown also differs at the back and at the front, as the maximum crown height is different; see Fig. 5a at $\tau = 10.3$. This causes the Worthington jet and splash to be directed against the direction of impact; see Fig. 5a at $\tau = 47.2$. For an oblique impact to be called a *90°-like* crown splash, the fingers do not have to emerge all around the crown and can only cover the front half of it. An example is shown in Fig. 5b. However, if the fingers are positioned at a distinct position at the side of the crown or the front middle only, this is characterized as another splashing type; see Section 3.3 and Section 3.4, respectively.

The trajectories of the secondary droplets are evaluated manually for a sample set of experiments from the three-perspective high-speed recordings. In the case of the Worthington splash, the droplets fly with an azimuth of $\varphi = 180°$ and an elevation of $30° \leq \theta \leq 90°$ depending on the impact angle. For the crown splash, the azimuth starts at $\varphi \leq 40°$ at lower Weber numbers, but it then opens up to all azimuth ($0° \leq \varphi \leq 180°$) with increasing We. The elevation is high with $40° \leq \theta \leq 80°$.

3.2. Threshold for 90°-like splashing

The threshold at which the 90°-like splashing (Worthington splash or crown splash) transitions to the next splashing type (side only splashing, blue in Fig. 4, and see Section 3.3) is only dependent on the impact angle α within the investigated range. The threshold is determined to $\alpha = 81°$, and it is plotted in Fig. 4 with a dashed red line.

At low Weber numbers, 90°-like splashing transitions to deposition, as observed for normal ($\alpha = 90°$) impacts. However, while Worthington splashing occurs at $\alpha = 90°$ and $We = 430$, deposition is observed at $\alpha = 83°$ for the same Weber number, see Fig. 4. This comparison suggests that the critical Weber number required for splashing increases as the impact angle decreases within the 90°-like splashing regime. Due to the limited data available in this region, no statistically valid threshold formulation could be derived.

3.3. Side-only splashing (SO)

The next splashing type is called *side-only* splashing (SO) (blue in Fig. 4). High-speed camera recordings of the side and front views as well as the side and top views are shown in Fig. 6. The rim remains stable in the early phase of the development of the asymmetric crown, $\tau \leq 5.5$ is this example. As the crown expands, instabilities arise on the sides of the crown which intensify to one finger at each side ($\tau = 10.9$

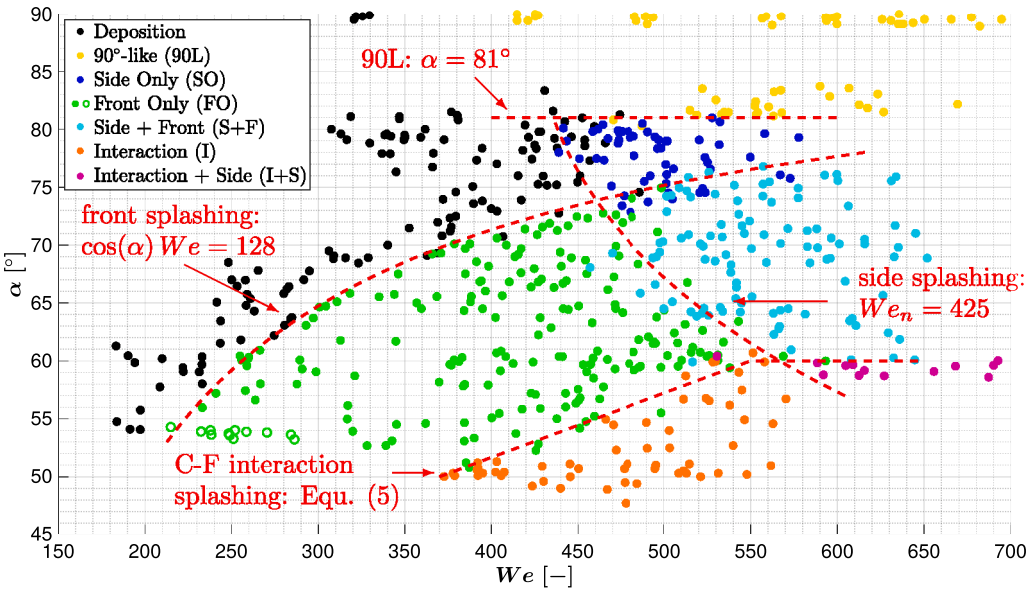

Fig. 4. Regime map of different observed splashing types (coloured dots) and threshold models (red dashed line) for $\delta = 0.22 \pm 0.02$, $Oh = 0.013 \pm 0.001$ in dependence of Weber number We and impact angle α.

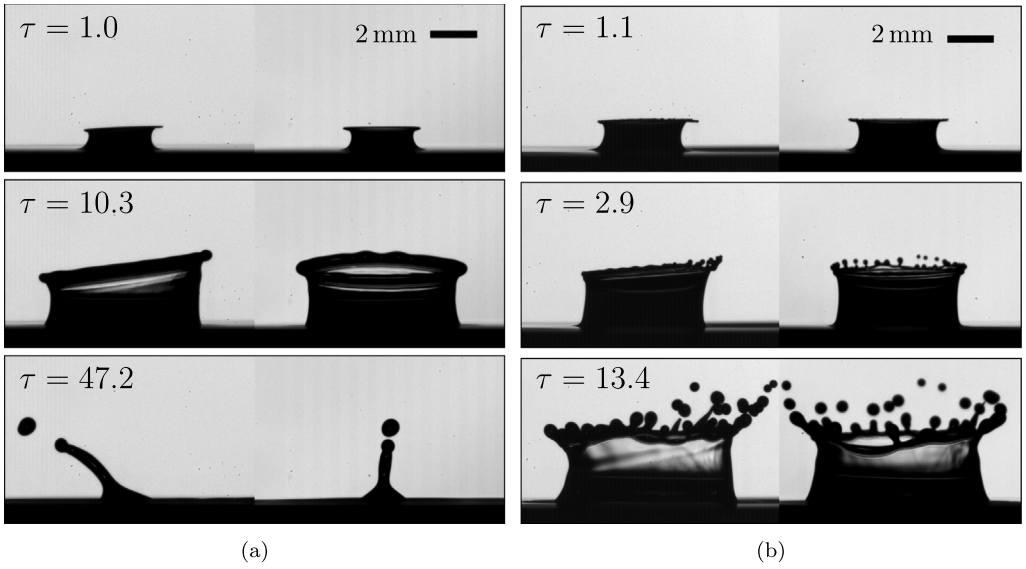

Fig. 5. Side and front views of two experiments of the 90°-like (90L) splashing type. (a) Worthington splash Exp. No. 1 in Table 2, $We = 553$, $\alpha = 82.4°$, (b) crown splash Exp. No. 2, $We = 703$, $\alpha = 81.8°$.

and $\tau = 15.2$). The position of the fingers is characteristic of this splashing type. These fingers grow, and one or two secondary droplets detach from each finger, which happens very symmetrically ($\tau = 17.9$). At the front, the rim is more stable; only a cusp or a finger can be seen, from which no secondary droplets detach. The development at the back part of the crown is different compared to in 90°-like splashing. First, the crown is bent inwards ($\tau = 0.8$, $\tau = 1.9$), which subsequently flips outwards ($\tau = 5.5$) and forms a cusp or a small finger ($\tau = 10.9$) as in the example in Fig. 6. This was described as *oblique mechanism of crown formation* in the numerical investigations of Stober et al. [25]. From the finger at the back of the crown, no secondary droplet is ejected.

Comparing the crown development of the side-only with the 90°-like splashing reveals one interesting correlation. The oblique mechanism of crown formation at the back of the crown is always present in the side-only splashing type, but it was never observed for the 90°-like splashing. The difference in early crown formation can be observed comparing the crown at the back in Fig. 5a ($\tau = 1.0$) with Fig. 6a ($\tau =$ 0.8). This suggests the following explanation for the side-only splashing: The occurrence of the oblique mechanism of crown formation leads to an uneven development of the crown that is dependent on the azimuthal position φ. At the back part of the impact, the oblique mechanism initially bends the crown inward before it flips outward. The rest of the crown develops regularly, pointing outward from the start. At the side of the crown, where the transition occurs between oblique and regular crown development, instabilities are introduced, and fingers are more likely to form. With that, the oblique mechanism promotes finger formation and secondary droplet ejection at the sides of the crown. If the impact angle is increased to a certain angle, the oblique mechanism of crown formation stops to occur and the crown develops with the same regular mechanism on the back as on the front. This, in contrast, leads to a uniform crown formation all around the crown (independent from the azimuth position), which leads to a stable rim during the entire impact process. No secondary droplets are ejected, and the crown falls back onto the film, which leads to Worthington

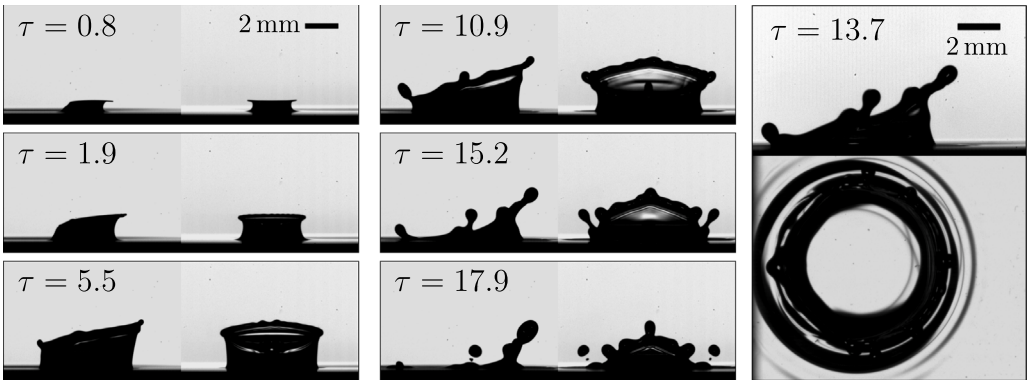

Fig. 6. Two experiments of the side-only (SO) splashing type. (a) Side and front views Exp. No. 3 in Table 2, $We = 489$, $\alpha = 75.5°$, (b) side and top views Exp. No. 4, $We = 478$, $\alpha = 76.3°$.

splashing (Fig. 5a). The threshold described in the last Section 3.2 is defined by the limiting angle for the oblique mechanism of crown formation to occur.

The trajectories of the secondary droplets are evaluated manually for a sample set of experiments from the three-perspective high-speed recordings. The elevation the ejected droplets for the side-only splashing type is around $0° \leq \theta \leq 50°$. The first droplets that detach have the highest elevations, which decrease to zero for the last secondary droplets or for low Weber numbers. The azimuth is completely different compared to in 90°-like splashing. It corresponds to the finger position in the crown and lies at $70° \leq \varphi \leq 120°$. With an increase in Weber number, the finger position and secondary droplets tend to shift to lower azimuthal angles φ.

3.4. Front-only splashing (FO)

The next phenomenon is front-only (FO) splashing, and it is marked with green dots in Fig. 4. Opposite to the side-only splashing type, the rim remains stable at the back and the side part of the crown while splashing occurs only at the front. Images from high-speed camera recordings of this splashing type are shown in Fig. 7.

An asymmetric crown with an initially stable rim forms. The crown on the front expands faster than on the side and back parts of it (Fig. 7b, $\tau = 2.4$). From the top view, it can be seen that the rim is not circular but has a higher curvature at the front, similar to an ellipse. The curvature of the rim at the front intensifies as the crown develops further and the rim grows into the crown sheet described by Taylor [32]. In this region of the highest rim curvature, a single central finger forms. This is similar to the formation of fingers from disturbances in the rim [33] as the rim grows perpendicular to its axis. If exactly one finger forms, this is called *single-finger front-only* splashing (sFO). The finger grows further with liquid from the rim and crown sheet supplying it and disintegrates into secondary droplets (Fig. 7a, $\tau = 15.9$) due to Rayleigh–Plateau instability [34]. The rim on the sides is more stable during the whole impact process. First, only a kink can be observed in the rim on the side (Fig. 7a, $\tau = 10.2$), which can grow to a cusp in the receding phase of the crown ($\tau > 10.2$). The position of the cusp corresponds to the positions of the fingers in the side-only splashing described above (Section 3.3), and it is caused by the oblique mechanism of crown formation present on the back. The crown's back side is initially bent inwards and subsequently flips outwards, which generates a cusp on the back side of the rim; see $\tau = 5.6$ in the present experiment. The single-finger front-only splashing morphology was described in an experimental study by Stober et al. [12].

For an increased Weber number, finger formation and splashing occur at earlier non-dimensional times τ, and the first fingers, as well as the first secondary droplets, are thinner. Beyond that, for higher Weber numbers, the forward rim starts to become wavy, and more than one finger can form close to each other at the front, which is shown in Fig. 8. As splashing starts earlier and from more fingers, significantly more secondary droplets are ejected. This variation in morphology with more than one finger is referred to as *multiple-finger front-only* splashing (mFO).

These observations match the findings about the We influence on secondary droplets for normal droplet impacts, [12,35,36]. A higher Weber number generally leads to more secondary droplets and splashing at earlier non-dimensional times τ. Furthermore, the early secondary droplets are smaller with increasing Weber and increase with non-dimensional time. The explanation for these phenomena is that a higher Weber number has a relatively higher kinetic energy and, therefore, leads to thinner crown and fingers as well as earlier splashing with smaller secondary droplets.

When the impact angle α is reduced, the crown formation at the front is hindered at early times, as shown in Fig. 9. Comparing $\tau = 0.6$ and $\tau = 1.4$ of this experiment with $\tau = 0.7$ for higher impact angles in Fig. 7 reveals these differences. At a later stage (Fig. 9, $\tau = 2.8$), a crown rises at the front, fingers grow ($\tau = 6.5$), and secondary droplets detach ($\tau = 16.2$). This crown development and splashing type is considered a low-impact angle version of front-only splashing. It is represented by blank green symbols in Fig. 4, highlighting its occurrence exclusively at low impact angles and low Weber numbers within the FO regime.

The trajectories of the secondary droplets ejected by the front-only splashing types are evaluated manually for a sample set of experiments. The secondary droplets fly approximately in azimuth $\varphi \approx 0°$ for the single-finger front-only type (sFO) and in a narrow range of $\varphi \leq 10°$ for the multiple-finger case (mFO). The azimuth angle range gets larger with higher Weber numbers because the number of fingers increases and the fingers are more spread. The elevation angle θ of the trajectory lies at $0° \leq \theta \leq 50°$. The elevation decreases for droplets that are ejected later.

3.5. Combination of side and front splashing (S+F)

The last two splashing types (SO and FO) can also occur combined (S+F). Secondary droplets detach from the characteristic fingers at the side of the crown and from fingers at the front, as shown in Fig. 10. At the back part of the crown, an oblique mechanism is present leading to a cusp or a finger, as for SO and FO.

This combined splashing type is marked by cyan dots in the regime map in Fig. 4. From the location relative to the side-only splashing (blue) and the front-only splashing (green), it seems that SO and FO can superpose to (S+F) without one phenomenon displacing the other. This in turn means that the mechanisms triggering the development of these splashing types do not interfere with one another. These three splashing

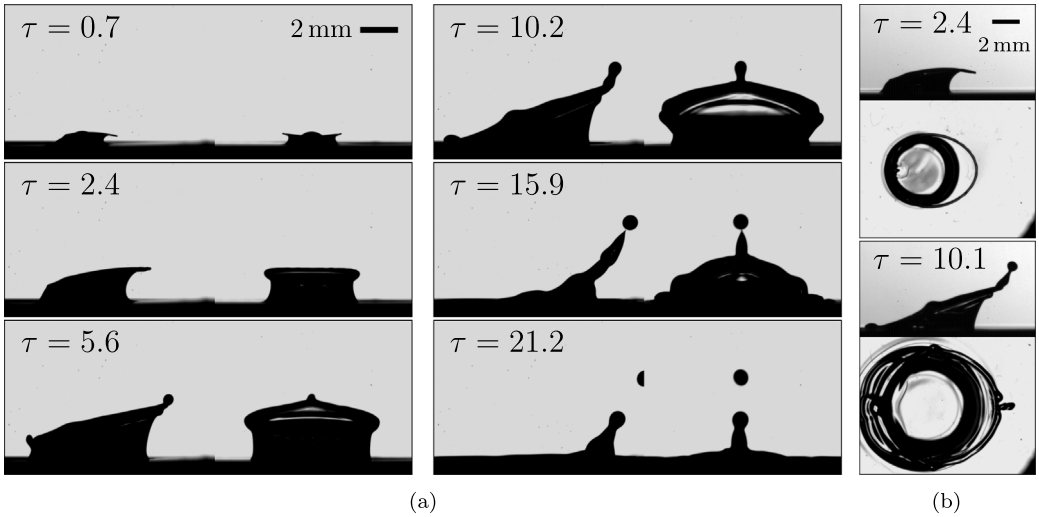

Fig. 7. Two experiments of the front-only (FO) splashing type with a single finger. (a) Side and front views Exp. No. 5 in Table 2, $We = 395$, $\alpha = 64.5°$, (b) side and top views Exp. No. 6, $We = 460$, $\alpha = 62.0°$.

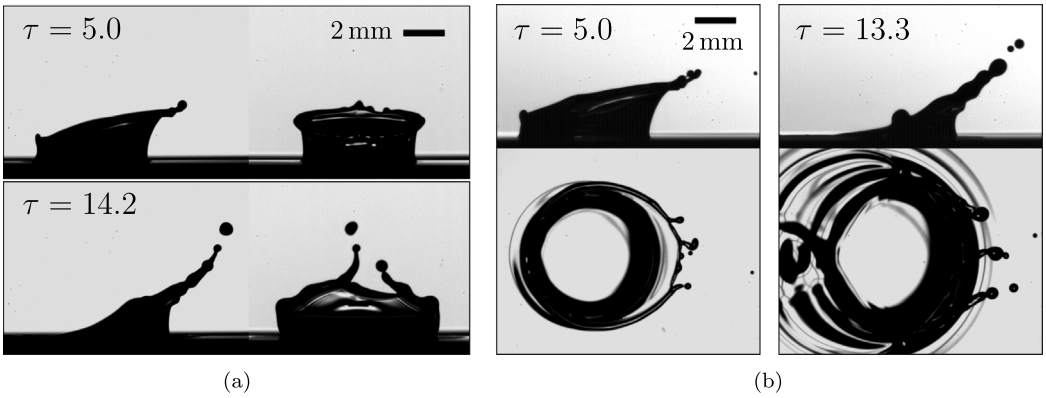

Fig. 8. Two experiments of the front-only (FO) splashing type with multiple fingers. (a) Side and front views Exp. No. 7 in Table 2, $We = 486$, $\alpha = 61.8°$, (b) side and top views Exp. No. 8, $We = 448$, $\alpha = 62.2°$.

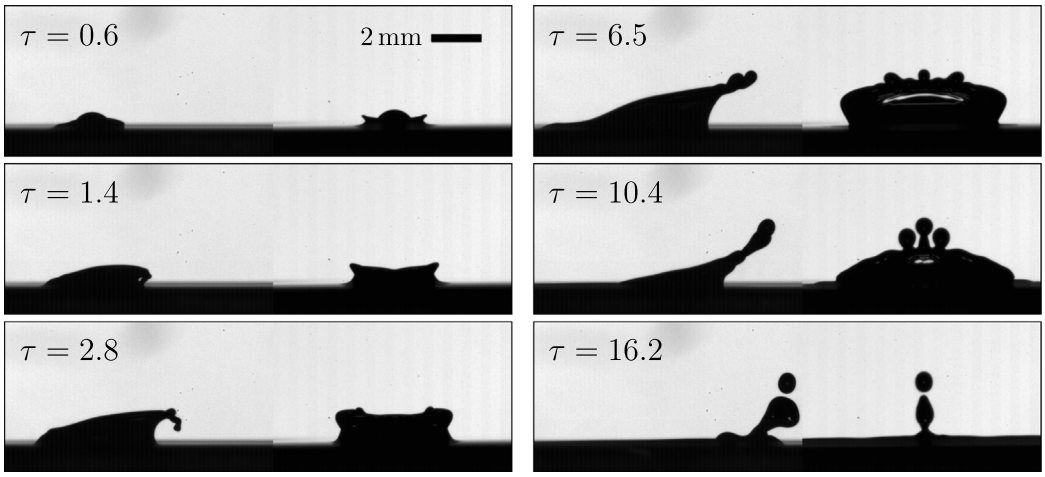

Fig. 9. Side and front views of front only splashing where the front crown formation is hindered. Exp. No. 9 in Table 2, $We = 284$, $\alpha = 53.6°$.

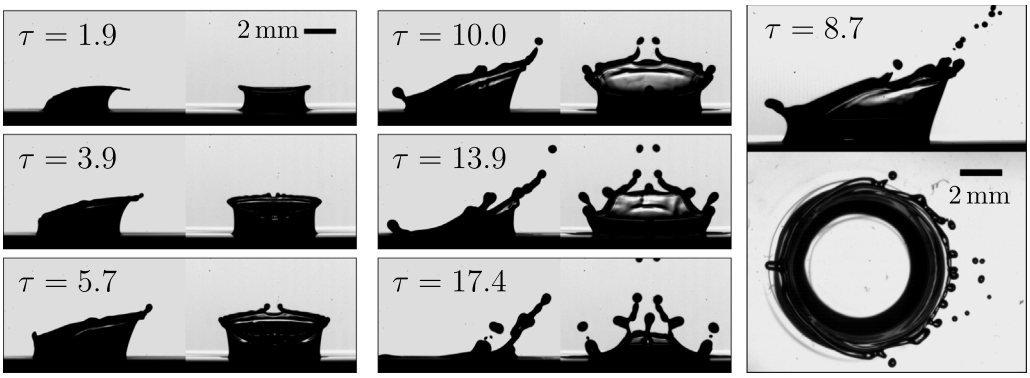

Fig. 10. Two experiments of the combined front and side splashing type (F+S). (a) Side and front views Exp. No. 10 in Table 2, $We = 539$, $\alpha = 67.6°$, (b) side and top views Exp. No. 11, $We = 601$, $\alpha = 70.0°$.

types (SO, FO, S+F) can therefore be described by two thresholds, one for side splashing and one for front splashing. The two thresholds are presented in the next two sections 3.6 and 3.7.

The trajectories of the secondary droplets are evaluated manually for a sample set of experiments from the three-perspective high-speed recordings and are a combination of the front-only and side-only splashing. Azimuth angles close to $\varphi \approx 0°$ and around $\varphi \approx 90°$ can be found with an elevation of $\theta \leq 50°$.

3.6. Threshold side splashing

Splashing from the side parts of the crown occurs in the SO regime (blue in Fig. 4), the S+F regime (cyan), as well as in the combination of crown film interaction with side splashing (I+S) (magenta) explained in Section 3.9. Side splashing can be observed if the Weber number is high enough, otherwise no droplets detach from the side parts of the crown, which then corresponds either to the deposition or the front-only splashing regime. For lower impact angles, a higher critical Weber number has to be overcome.

A threshold in the α-We space can be generally mathematical expressed by $f(\alpha, We) = c$, with f an arbitrary function of α and We, and the constant c. Instead of using the impact angle α directly, $\sin(\alpha)$ seems to be a meaningful physical parameter for this threshold, as it expresses the ratio of the normal impact velocity to the total velocity ($\sin(\alpha) = U_n/U$); compare Fig. 2. An adapted power law approach ($\sin(\alpha)^p We = c$) was used, and a least-square fitting provided the parameters $p \approx 2$ and $c \approx 425$. These results are particularly interesting, as the threshold formulation can be rewritten into

$$\sin(\alpha)^2 We = We_n = 425. \tag{1}$$

This firstly confirms the choice of $\sin(\alpha)$, and secondly, the exponent $p = 2$ reveals that side splashing is only dependent on the normal Weber number We_n, which is built with the velocity component normal to the wall film. The normal Weber number is the correct and sole physical quantity to describe the onset of splashing on the side parts of the crown, independent of the impact angle or any tangential velocity component. This means that the tangential component of the impact does not promote or hinder side splashing, as it does not contribute any momentum to the development of the crown to the sides. The validity range of this threshold lies at $58° \leq \alpha \leq 81°$, as side splashing occurs only in this range and the threshold was fitted for this range.

The regime border for side splashing has a transition area where side splashing and no side splashing can be observed; see Fig. 4. It has a width in the Weber number of approximately ± 20, which is about as large as the measurement uncertainty for the Weber number. The threshold of $We_n = 425$ is plotted in Fig. 4 and fits well with the observed phenomena.

3.7. Threshold front splashing

Front splashing includes the FO regime (green in Fig. 4) and the (S+F) regime in cyan. It occurs in an impact angle range $54° \leq \alpha \leq 77°$ if the Weber number is high enough to overcome deposition. The Weber number needed for splashing increases with increasing impact angle. This in turn means that if the impact angle α is increased at constant We, front splashing transitions to deposition or to splashing occurring only at the side part of the crown.

A similar approach for a threshold formulation was chosen. This time, the $\cos(\alpha)$ is expected to be a relevant physical quantity, as it describes the tangential portion of the total impact velocity ($\cos(\alpha) = U_t/U$). The modified power law approach is then ($\cos(\alpha)^p We = c$). A least square optimization provides $p = 0.99$ and $c = 128$. Setting the exponent p to $p = 1.0$, the threshold can be written in the following forms,

$$\cos(\alpha)\, We = 128, \tag{2}$$

and

$$\sqrt{We_t\, We} = 128 \tag{3}$$

with the tangential Weber number We_t, as defined in the introduction Section 1. The first way of writing the threshold (Eq. (2)) is intuitive, as it directly contains the physical quantities of the axis of the regime map, the total Weber number We, and the impact angle α. The exponent $p = 1$ reveals that the ratio of the tangential impact velocity to the total velocity is the crucial physical quantity to define the onset of front splashing. This also corresponds to the ratio of the tangential momentum I_t to the total momentum I of the impacting droplet.

$$\cos(\alpha) = \frac{U_t}{U} = \frac{I_t}{I} \tag{4}$$

It is, therefore, the portion of the tangential momentum that promotes front splashing.

The alternative formation (Eq. (3)) represents a geometric mean of the tangential We_t and the total Weber number We. This illustrates that the tangential as well as the total Weber number contribute equally to the ejection of droplets from the front part of the crown. The validity range of this threshold lies at $54° \leq \alpha \leq 77°$, as front splashing occurs only in this range, and the threshold was fitted for this range.

3.8. Interaction of the crown with the film (I)

Another distinct phenomenon that was observed in the investigated impact parameter range is the *interaction of the crown with the wall film* (I), marked with orange dots in the regime map (Fig. 4), and stills from high-speed recordings are shown in Fig. 11. In the early

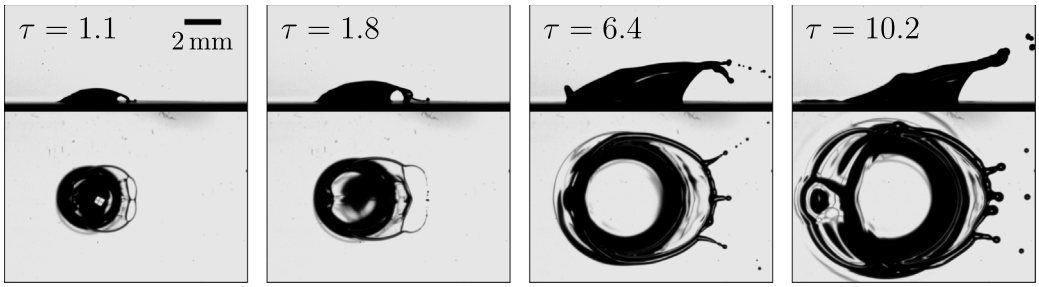

Fig. 11. Side and top views of the interaction of the crown with the wall film. Exp. No. 12 in Table 2, $We = 469$, $\alpha = 54.2°$.

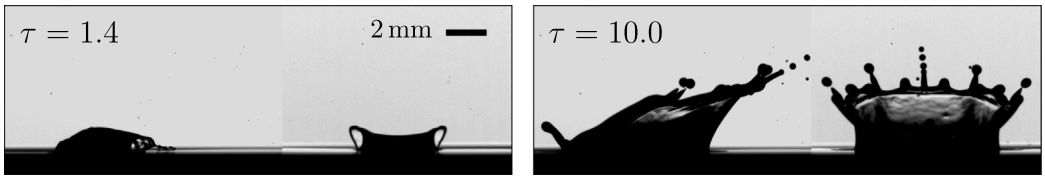

Fig. 12. Side and front views of the interaction of the crown with the wall film in combination with side splashing. Exp. No. 13 in Table 2, $We = 656$, $\alpha = 59.1°$.

crown formation phase ($\tau \approx 1.0$), the crown at the front touches (soft interaction) or collides (intense interaction) with the wall film. This introduces additional disturbances into the crown and rim which lead to multiple fingers and secondary droplets in the azimuth φ area of the interaction. The interaction can also lead to a rupture of the crown sheet and a prompt disintegration of the rim, producing tiny secondary droplets; see $\tau = 1.8$ in Fig. 11. Subsequently, a new rim forms and multiple fingers are generated; see $\tau = 6.4$. Many secondary droplets are ejected much earlier than for the other splashing types. The fingers as well as the secondary droplets are smaller in diameter. In case of an intense interaction (collision) of the crown with the wall film, the crown promptly ruptures, and liquid from the film is dragged with it. This generates even more and smaller secondary droplets and is observed for lower impact angles α and higher We. The phenomenon of crown-film interaction was described by Stober et al. [12]. The trajectories of the secondary droplets are very low and directed to the front. They lie in the range of $\varphi \leq 30°$ azimuth and $0° \leq \theta \leq 40°$ elevation, evaluated manually for a sample set of experiments.

3.9. Combination of crown-film interaction and side splashing (I+S)

Crown-film interaction (I) is also observed in a combination with splashing from the side fingers. This combined splashing regime (I+S) is plotted in magenta in Fig. 4. An example of this splashing type is presented in Fig. 12. The crown-film interaction at the front only affects the front part of the crown, while the fingers at the side can develop independently from it. This leads to a superposition of regimes without one displacing the other. The secondary droplets fly in the trajectory of the crown-film interaction as well as for the side-only phenomenon.

3.10. Threshold interaction of the crown with the film (I)

The interaction of the crown with the wall film was observed only for high Weber numbers and low impact angles; see the orange and magenta representation in Fig. 4. If We is not high enough or α is not small enough, the crown does not touch the wall film, and regular front splashing is observed. To describe this threshold, no power law approach was chosen, as the threshold covers a relatively small corner of the investigated parameter space, which limits the data's meaningfulness. However, two statements can be made from the dataset: First, crown-film interaction was observed only for $\alpha \leq 60°$, and second, the Weber number at which the interaction of the crown starts to occur decreases with decreasing α. The threshold is therefore defined accordingly by two linear functions as plotted in Fig. 4. It consists of a linear function from $\alpha = 50°$, $We = 370$ to $\alpha = 60°$, $We = 550$ and continued by a constant function $\alpha = 60°$ for $We \geq 550$,

$$\alpha = f(We) = \begin{cases} \frac{1°}{18} We + 29.4° & 370 < We < 550 \\ 60° & 550 \leq We \leq 650. \end{cases} \tag{5}$$

It is defined within $370 \leq We \leq 650$, as in that range, the transition from crown-film collision to regular crown development is observed.

4. Summary and conclusion

In this study, we experimentally investigated the oblique impact of an isopropanol droplet on a thin, horizontal, and quiescent wall film of the same liquid. By systematically varying the impact angle and Weber number, we addressed several open questions in the existing literature about crown formation, splashing types, and threshold models.

First, we provided a detailed description of crown morphology and splashing during oblique droplet impacts. Under certain conditions, secondary droplets can be ejected solely from either the side part or the front part of the crown. Additionally, splashing could result from interactions between the early crown and the wall film, or develop similarly to normal impacts on thin films. Combinations of these splashing types were also identified, such as combined side and front splashing, or side splashing coupled with crown-film interaction. The triggering mechanisms for these splashing types to develop do not interfere with one another, allowing a superposition and the overlap of multiple regimes without one displacing the other. Differentiating between these splashing types is crucial because the resulting secondary droplets vary significantly in size and trajectory.

Second, we presented a regime map and derived models to describe the borders of these splashing regimes. A power-law fit for the side splashing threshold revealed that it can be modelled using only the wall-normal Weber number with $We_n = 425$. The tangential Weber number does not promote or hinder splashing from the sides of the crown. Furthermore, the oblique mechanism of crown formation on the back was found to introduce disturbances to the rim on the side, promoting side splashing. When the impact angle exceeds $\alpha > 81°$, the oblique mechanism disappears, which marks the transition to the regime that corresponds to $\alpha = 90°$ impacts. The threshold for front splashing is described by $\cos(\alpha)\, We = 128$, indicating that the ratio of tangential impact momentum to total momentum ($\cos(\alpha)$) is the physical parameter driving front splashing, in addition to the Weber number. The threshold for crown-film interaction lies below $\alpha \leq 60°$,

with $We > 550$ for $\alpha = 60°$ and $We > 370$ for $\alpha = 50°$, approximated by a linear threshold in between.

These findings significantly enhance understanding of oblique droplet impacts, particularly the effect of impact angle and Weber number on the resulting crown development and splashing dynamics. The proposed regime map and threshold formulations provide valuable tools for predicting impact outcomes. Additionally, the detailed experimental recordings of crown development serve as a large dataset for the validation of numerical simulations.

CRediT authorship contribution statement

Jonathan Lukas Stober: Writing – original draft, Writing – review & editing, Visualization, Validation, Methodology, Investigation, Formal analysis, Data curation, Conceptualization. **Maurizio Santini:** Writing – review & editing, Supervision, Conceptualization. **Kathrin Schulte:** Writing – review & editing, Supervision, Funding acquisition, Conceptualization.

Funding

The authors wish to thank Deutsche Forschungsgemeinschaft (DFG), Germany for financial support in the framework of project GRK 2160/2 “Droplet Interaction Technologies” (DROPIT), under project number 270852890.

Declaration of competing interest

The authors declare that they have no known competing financial interests or personal relationships that could have appeared to influence the work reported in this paper.

Data availability

Data will be made available on request.

References

[1] R. Xu, G. Wang, P. Jiang, Spray cooling on enhanced surfaces: A review of the progress and mechanisms, J. Electron. Packag. 144 (1) (2021) http://dx.doi.org/10.1115/1.4050046.

[2] S. Kaiser, O. Schmitz, P. Ziegler, H. Klingels, The water-enhanced turbofan as enabler for climate-neutral aviation, Appl. Sci. 12 (23) (2022) 12431, http://dx.doi.org/10.3390/app122312431.

[3] F. Chang, H. Luo, C. Zhai, Y. Jin, P. Xiong, J. Wang, B. Song, J. Zhang, K. Nishida, Experimental investigation of fuel adhesion from wall-impinging spray with various injection mass ratios, Exp. Therm. Fluid Sci. 163 (2025) 111403, http://dx.doi.org/10.1016/j.expthermflusci.2024.111403.

[4] G.E. Cossali, A. Coghe, M. Marengo, The impact of a single drop on a wetted solid surface, Exp. Fluids 22 (6) (1997) 463–472, http://dx.doi.org/10.1007/s003480050073.

[5] C. Mundo, M. Sommerfeld, C. Tropea, Droplet-wall collisions: Experimental studies of the deformation and breakup process, Int. J. Multiph. Flow 21 (2) (1995) 151–173, http://dx.doi.org/10.1016/0301-9322(94)00069-V.

[6] R. Rioboo, C. Bauthier, J. Conti, M. Voué, J. De Coninck, Experimental investigation of splash and crown formation during single drop impact on wetted surfaces, Exp. Fluids 35 (6) (2003) 648–652, http://dx.doi.org/10.1007/s00348-003-0719-5.

[7] R.L. Vander Wal, G.M. Berger, S.D. Mozes, Droplets splashing upon films of the same fluid of various depths, Exp. Fluids 40 (1) (2006) 33–52, http://dx.doi.org/10.1007/s00348-005-0044-2.

[8] R.D. Deegan, P. Brunet, J. Eggers, Complexities of splashing, Nonlinearity 21 (1) (2008) C1–C11, http://dx.doi.org/10.1088/0951-7715/21/1/c01.

[9] A. Worthington, A Study of Splashes, Longmans, Green, and Co, London, 1908.

[10] T. Okawa, T. Shiraishi, T. Mori, Effect of impingement angle on the outcome of single water drop impact onto a plane water surface, Exp. Fluids 44 (2) (2008) 331–339, http://dx.doi.org/10.1007/s00348-007-0406-z.

[11] M. Bao, F. Wang, L. Gong, Y. Guo, S. Shen, Experimental study of different shape droplet oblique impact on a thin liquid film, Desalination Water Treat. 270 (2022) 35–43, http://dx.doi.org/10.5004/dwt.2022.28767.

[12] J.L. Stober, M. Santini, K. Schulte, Influence of Weber number on crown morphology during an oblique droplet impact on a thin wall film, Fluids 8 (11) (2023) 301, http://dx.doi.org/10.3390/fluids8110301.

[13] M.V. Gielen, P. Sleutel, J. Benschop, M. Riepen, V. Voronina, C.W. Visser, D. Lohse, J.H. Snoeijer, M. Versluis, H. Gelderblom, Oblique drop impact onto a deep liquid pool, Phys. Rev. Fluids 2 (8) (2017) http://dx.doi.org/10.1103/physrevfluids.2.083602.

[14] G. Liang, Y. Guo, Y. Yang, N. Zhen, S. Shen, Spreading and splashing during a single drop impact on an inclined wetted surface, Acta Mech. 224 (12) (2013) 2993–3004, http://dx.doi.org/10.1007/s00707-013-0910-6.

[15] J.J. Chen, Q.F. Liu, F. Zhang, F.L. Zhao, J.Y. Qu, Experimental investigation on water droplet impacting liquid film on inclined wetted surface, IOP Conf. Ser.: Earth Environ. Sci. 701 (1) (2021) 012005, http://dx.doi.org/10.1088/1755-1315/701/1/012005.

[16] X. Gao, R. Li, Impact of a single drop on a flowing liquid film, Phys. Rev. E 92 (2015) 053005, http://dx.doi.org/10.1103/PhysRevE.92.053005.

[17] Z. Che, A. Deygas, O.K. Matar, Impact of droplets on inclined flowing liquid films, Phys. Rev. E 92 (2) (2015) http://dx.doi.org/10.1103/physreve.92.023032.

[18] H. Kittel, Drop Impact onto a Wall Wetted by a Thin Film of Another Liquid (Ph.D. thesis), Technische Universität Darmstadt, 2019.

[19] L. Shan, Y. Song, S. Zhou, G. Liang, Experimental and numerical study of droplet impact on radially flowing liquid film, Ind. Eng. Chem. Res. 62 (4) (2023) 2008–2020, http://dx.doi.org/10.1021/acs.iecr.2c03821.

[20] I.T. Adebayo, O.K. Matar, Droplet impact on flowing liquid films with inlet forcing: The splashing regime, Soft Matter. 13 (41) (2017) 7473–7485, http://dx.doi.org/10.1039/c7sm01468f.

[21] G. Liang, L. Li, L. Chen, S. Zhou, S. Shen, Impact of droplet on flowing liquid film: Experimental and numerical determinations, Int. Commun. Heat Mass Transfer 126 (2021) 105459, http://dx.doi.org/10.1016/j.icheatmasstransfer.2021.105459.

[22] P. Brambilla, A. Guardone, Assessment of dynamic adaptive grids in volume-of-fluid simulations of oblique drop impacts onto liquid films, J. Comput. Appl. Math. 281 (2015) 277–283, http://dx.doi.org/10.1016/j.cam.2014.12.030.

[23] Y. Wu, B. Kong, B. Tong, Y. Xiao, G. Zhang, X. Hu, Oblique impact of droplet on a moving film in spray cooling, Eur. J. Mech. B Fluids 100 (2023) 21–36, http://dx.doi.org/10.1016/j.euromechflu.2023.02.002.

[24] Y. Cao, J. Wang, C. Zhu, Numerical simulation of microscale oblique droplet impact on liquid film, Aerospace 10 (2) (2023) 119, http://dx.doi.org/10.3390/aerospace10020119.

[25] J.L. Stober, J. Potyka, M. Ibach, B. Weigand, K. Schulte, DNS of the early phase of oblique droplet impact on thin films with FS3D, 2023, arXiv:2311.17690, URL https://arxiv.org/abs/2311.17690.

[26] H. Ding, X. Chai, X. Song, Y. Yang, C. Wen, Asymmetrical morphological evolution and energy conversion of droplets impacting on the moving film, Phys. Fluids 37 (2) (2025) http://dx.doi.org/10.1063/5.0244521.

[27] Z. Chen, C. Shu, Y. Wang, L. Yang, Oblique drop impact on thin film: Splashing dynamics at moderate impingement angles, Phys. Fluids 32 (3) (2020) 033303, http://dx.doi.org/10.1063/5.0004142.

[28] J. Steigerwald, M. Ibach, J. Reutzsch, B. Weigand, Towards the numerical determination of the splashing threshold of two-component drop film interactions, High Perform. Comput. Sci. Eng. rq 20 (2021) 261–279, http://dx.doi.org/10.1007/978-3-030-80602-6_17,

[29] M. Santini, G.E. Cossali, M. Marengo, Device and method for drops generation, 2008, WO 2010/021004 A1, PCT/IT2008/000554, 22 August 2008.

[30] A.K. Ruprecht, C. Pruss, H.J. Tiziani, W. Osten, P. Lucke, A. Last, J. Mohr, P. Lehmann, Confocal micro-optical distance sensor: Principle and design, in: Optical Measurement Systems for Industrial Inspection IV, vol. 5856, SPIE, 2005, pp. 128–135.

[31] Dortmund Data Bank, 2024, URL https://www.ddbst.com. (Accessed: 27 November 2024).

[32] G.I. Taylor, The dynamics of thin sheets of fluid. III. Disintegration of fluid sheets, Proc. Royal Soc. London 253 (1274) (1959) 313–321, http://dx.doi.org/10.1098/rspa.1959.0196.

[33] I.V. Roisman, C. Tropea, Impact of a drop onto a wetted wall: Description of crown formation and propagation, J. Fluid Mech. 472 (2002) 373–397, http://dx.doi.org/10.1017/s0022112002002434.

[34] L. Rayleigh, On the instability of jets, Proc. Lond. Math. Soc. 10 (1878) 4–13.

[35] G. Cossali, M. Marengo, A. Coghe, S. Zhdanov, The role of time in single drop splash on thin film, Exp. Fluids 36 (2004) 888–900, http://dx.doi.org/10.1007/s00348-003-0772-0.

[36] T. Okawa, T. Shiraishi, T. Mori, Production of secondary drops during the single water drop impact onto a plane water surface, Exp. Fluids 41 (2006) 965–974, http://dx.doi.org/10.1007/s00348-006-0214-x.